

ON THE OPTIMAL CONTROL OF THE SCHLÖGL-MODEL ^{*}

RICO BUCHHOLZ[†], HARALD ENGEL[‡], EILEEN KAMMANN[§], AND FREDI TRÖLTZSCH[¶]

Abstract. Optimal control problems for a class of 1D semilinear parabolic equations with cubic nonlinearity are considered. This class is also known as the Schlögl model. Main emphasis is laid on the control of traveling wave fronts that appear as typical solutions to the state equation.

The well-posedness of the optimal control problem and the regularity of its solution are proved. First-order necessary optimality conditions are established by standard adjoint calculus. The state equation is solved by the implicit Euler method in time and a finite element technique with respect to the spatial variable. Moreover, model reduction by Proper Orthogonal Decomposition is applied and compared with the numerical solution of the full problem. To solve the optimal control problems numerically, the performance of different versions of the nonlinear conjugate gradient method is studied. Various numerical examples demonstrate the capacities and limits of optimal control methods.

AMS subject classification.

Key words. Schlögl model, semilinear parabolic equation, travelling wave front, optimal control, model reduction

1. Introduction. In this paper, we consider the numerical treatment of a class of optimal control problems for a semilinear parabolic equation with non-monotone polynomial nonlinearity and discuss some associated questions of mathematical analysis. In the applications, the problem is related to controlled reaction-diffusion processes, where wave type solutions appear that should be influenced in a desired way. We investigate the following optimal control problem:

Minimize the objective functional

$$J := \frac{c_Q}{2} \iint_Q (u(x,t) - u_Q(x,t))^2 dxdt + \frac{c_T}{2} \int_{\Omega} (u(x,T) - u_T(x))^2 dx + \frac{\lambda}{2} \iint_Q f^2(x,t) dxdt \quad (1.1)$$

subject to the state equation

$$\begin{aligned} u_t(x,t) - u_{xx}(x,t) + R(u(x,t)) &= b(x,t) f(x,t) && \text{in } Q \\ u(x,0) &= u_0(x) && \text{in } \Omega \\ u_x(0,t) = u_x(L,t) &= 0 && \text{in } (0,T) \end{aligned} \quad (1.2)$$

and possibly to pointwise box constraints

$$f \in F_{ad} := \{f \in L^\infty(Q) \mid f_a \leq f(x,t) \leq f_b \text{ for a.a. } (x,t) \in Q\}. \quad (1.3)$$

In this setting, positive numbers T and L , non-negative numbers λ, c_Q, c_T and numbers $f_a < f_b$ are given, where we allow the values $f_a = -\infty$ and $f_b = \infty$. Moreover, functions $b \in L^\infty(Q), u_0 \in$

^{*}This work was supported by DFG in the framework of the Collaborative Research Center Sfb 910, project B6.

[†]Physikalisches Institut, Universität Bayreuth, D-95447 Bayreuth, Germany (rico.buchholz@uni-bayreuth.de).

[‡]Institut für Theoretische Physik, Technische Universität Berlin, D-10623 Berlin, Germany (Harald.engel@physik.tu-berlin.de).

[§]Institut für Mathematik, Technische Universität Berlin, D-10623 Berlin, Germany (eileen.kammann@googlemail.com).

[¶]Institut für Mathematik, Technische Universität Berlin, D-10623 Berlin, Germany (troeltzsch@math.tu-berlin.de).

$L^\infty(\Omega), u_T \in L^2(\Omega), u_Q \in L^2(Q)$ are given. Here and throughout this paper, we use the notation $\Omega = (0, L), Q = \Omega \times (0, T), \Sigma = \{0, L\} \times (0, T)$. The function b can be used to select a subdomain of Q , where the control f is acting.

The nonlinearity in the parabolic equation is defined by a cubic reaction term $R : \mathbb{R} \rightarrow \mathbb{R}$ of the form

$$R(u) = k(u - u_1)(u - u_2)(u - u_3)$$

with real numbers $k \geq 0$ and $u_1 < u_2 < u_3$. In particular, we are interested in the important case

$$R(u) = k u^3 - a u,$$

with a positive number a . All of our computations are performed with the associated simplified state equation

$$\begin{aligned} u_t(x, t) - u_{xx}(x, t) + k u^3(x, t) - a u(x, t) &= b(x, t) f(x, t) && \text{in } Q \\ u(x, 0) &= u_0(x) && \text{in } \Omega \\ u_x(0, t) = u_x(L, t) &= 0 && \text{in } (0, T), \end{aligned} \tag{1.4}$$

where R can be written as $R(u) = k u^3 - a u = k u (u - \sqrt{a/k})(u + \sqrt{a/k})$. In what follows, u is said to be the state of the system, while f is the control (forcing) function.

In Physics, the equation (1.2) is known under the name "Schlöggl model" and there is an extensive literature devoted to the behavior of its solutions. We refer, for instance, to Schlöggl [28] or the exposition in [24].

In the theory of partial differential equations, the equation (1.2) belongs to the class of semilinear parabolic equations. Meanwhile, many papers were published on associated optimal control problems and the corresponding numerical analysis is already very well investigated. For instance, first-order necessary optimality conditions in form of the Pontryagin maximum principle were presented by Casas [5], Bonnans and Casas [3] or Raymond and Zidani [27]. First-order optimality conditions of Karush-Kuhn-Tucker type are the subject of many other papers, we just mention the textbook by the third author [31] and the book by Hinze et al. [14] that in particular contains details on numerical methods. We also mention an early paper on the numerics for the optimal control of semilinear equations with Stefan-Boltzmann boundary conditions by Heinkenschloss and Sachs [12], where the state appears with power 4 in the boundary condition.

Second-order sufficient optimality conditions were also studied, we mention one of the latest papers by Casas et al. [6], where also state-constraints are admitted. More recently, the error analysis for the numerical approximation of such problems became an active field of research, see [22], where also an impressive survey on the whole field is given. In [31] and [14], the reader may find an extensive list of further references.

In contrast to the papers mentioned above, the nonlinear function R is not monotone. Therefore, the theory of existence and regularity of solutions to semilinear parabolic equations of [5] or [27] cannot be directly applied to (1.4). Closing this gap is, together with a result on H^2 -regularity, some new contribution of our paper to the theory of optimal control of PDEs. However, this does not go much beyond the known theory.

Our interest in the particular optimal control problem (1.1)-(1.3) has another reason; this is the occurrence of wave type solutions of (1.4) for suitable initial data and $f = 0$. These solutions

are functions u of the type $u(x,t) = z(x - ct)$ that behave like traveling waves with velocity c . For the nonlinearity $R(u) = (u - u_1)(u - u_2)(u - u_3)$ and $f = 0$, the parabolic equation of (1.4) admits three constant functions as solutions, namely $u(x,t) \equiv u_i$, $i = 1, 2, 3$. The values u_i are the fixed points of the dynamical system (1.4). Two of them, u_1 and u_3 are stable. Solutions with initial data close to u_i converge to u_i as $t \rightarrow \infty$. The value u_2 , however, is unstable.

Wave type solutions for reaction-diffusion equations constitute an interesting topic that was extensively studied in literature. We mention only the textbooks by Kuramoto [21], Murray [26] or Smoller [30]. Moreover, there are many contributions to the control of such equations in the context of Physics, we refer exemplarily to Schöll and Schuster [29]. Some associated optimal control problems have also been considered in the mathematical community of PDE control. We refer to Borzi and Griesse [4], who considered the optimal control of λ - ω -systems, where spiral waves may occur. Moreover, we mention Kunisch and Wagner [18], [19], [20], and Kunisch et al. [17], who discuss monodomain or bidomain equations playing an important role in heart medicine.

Controlling wave type solutions is numerically challenging in general. We observed this already for the 1D Schlögl model, where the presence of the unstable fixed point u_2 might cause the difficulties we observed. Numerical iteration methods of optimization turned out to be much slower and less stable than for parabolic equations with monotone nonlinearity, say for a semilinear heat equation with monotone nonlinearity as in Kammann et al. [15].

The report on our numerical experience in controlling traveling wave fronts and the variety of associated numerical examples with nice geometrical interpretation constitute the main novelty of our paper. As mentioned above, we also address some aspects of analysis for the problem (1.1)–(1.3). First, we investigate existence, uniqueness and regularity of solutions to the state equation by transforming the state equation to one with monotone nonlinearity. Then the solvability of the optimal control problem is an immediate consequence. For the convenience of the reader, we also survey some known results on the Schlögl model and on wave type solutions that are well known in the relevant literature in Physics.

Next, we discuss the numerical optimization by nonlinear conjugate gradient methods for several types of optimal control problems: We study the stopping of a traveling wave front at a certain time for a problem that in physics is called nucleation. Moreover, we discuss other objectives such as acceleration of traveling wave fronts or steering them to one of the steady states. The treatment of such problems by optimal control methods seems to be new.

Another issue is the performance of POD, a standard method of model order reduction that turned out to be very efficient for many classes of parabolic control problems. We observed that a greater number of basis functions is needed than for the semilinear heat equation with monotone nonlinearity. This behavior was also observed by M. Müller in his thesis [25].

Let us comment already here on the solvability of the optimal control problem related to the choice of regularization parameter λ . Suppose that we take $\lambda = 0$ and that the box constraints (1.3) are missing. Assume that we can compute a control function $f \in L^2(Q)$ such that $u = u_Q$ holds for the associated state u . Then the desired state u_Q can be exactly reached, i.e. we are able to exactly follow the desired trajectory u_Q . If $u_T = u(x,T)$ holds as well, then the objective functional has the optimal value zero. In this case, this control f is optimal and hence the optimal control problem was solvable.

Unfortunately, it is often difficult to predict whether u_Q can be exactly reached or not. If not, then the optimal control problem (1.1)–(1.2) will most likely be unsolvable for $\lambda = 0$ without control constraints. This problem can be avoided by the choice $\lambda > 0$ or by adding the box constraints

(1.3). Then our problem is solvable, even if u_Q cannot be reached exactly.

2. The optimal control problem and first-order optimality conditions.

2.1. Well-posedness of the optimal control problem. We start by the well-posedness of the state equation (1.2). In the associated result that is formulated below, we use the standard Sobolev space $W(0,T) = L^2(0,T,H^1(\Omega)) \cap H^1(0,T;H^1(\Omega)')$.

THEOREM 2.1. *Suppose that it holds $k \geq 0$ and $u_1 < u_2 < u_3$. Then, for all $f \in L^2(Q)$ and $u_0 \in L^\infty(\Omega)$, the state equation (1.2) has a unique solution u in $L^\infty(Q) \cap W(0,T) \cap C([0,L] \times (0,T])$. If $u_0 \in C[0,1]$, then the solution is continuous even on $[0,1] \times [0,T]$. The mappings $f \mapsto u$ and $f \mapsto u(\cdot, T)$ are continuously Fréchet differentiable from $L^2(Q)$ to $W(0,T) \cap L^\infty(Q)$ and to $C(\bar{\Omega})$, respectively.*

Proof. For $R(u) = k(u - u_1)(u - u_2)(u - u_3)$, the derivative R' is a polynomial of even order that is bounded from below by some constant $C < 0$. Define $\mu = |C|$. Then the function

$$\tilde{R}(u) := R(u) + \mu u$$

is monotone non-decreasing. This observation is the reason for the following transformation: We define

$$u(x,t) := e^{\mu t} v(x,t).$$

Inserting this expression in (1.2), we obtain after an easy calculation the equation

$$e^{\mu t} v_t - e^{\mu t} v_{xx} + R(e^{\mu t} v) + e^{\mu t} \mu v = b f,$$

and hence the system

$$\begin{aligned} v_t(x,t) - v_{xx}(x,t) + e^{-\mu t} R(e^{\mu t} v) + \mu v &= e^{-\mu t} b(x,t) f(x,t) && \text{in } Q \\ v(x,0) &= u_0(x) && \text{in } \Omega \\ v_x(0,t) = v_x(L,t) &= 0 && \text{in } (0,T). \end{aligned} \tag{2.1}$$

For each fixed t , the function $v \mapsto e^{-\mu t} R(e^{\mu t} v) + \mu v$ is monotone non-decreasing and differentiable. Moreover, it is continuous w.r. to t for all fixed v . Therefore, the monotonicity and Carathéodory conditions are satisfied that are needed for existence and uniqueness of a solution v . Since $\Omega = (0,L)$ is one-dimensional, the equation (2.1) admits for each $f \in L^2(Q)$ and $u_0 \in L^\infty(0,L)$ a unique solution $v \in L^\infty(Q) \cap W(0,T) \cap C([0,L] \times (0,T])$. For $u \in C[0,L]$ we even have $v \in C([0,L] \times [0,T])$. For this result on existence, uniqueness and regularity, we refer to Casas [5], Raymond and Zidani [27] or to the exposition in [31], Theorem 5.5. Associated with v , we also obtain a unique solution u with the same regularity as v . The claimed differentiability is also standard for parabolic problems with monotone nonlinearity, see e.g. [31], Theorem 5.9. \square

Let us mention here a hidden difficulty: For $f \in L^2(Q)$, the boundedness of the solution u is only granted in one-dimensional domains as in our case. If the spatial domain is of dimension greater than one, then we would need control constraints to have control functions f of higher integrability, say $f \in L^\infty(Q)$ to achieve continuity of u . Without such constraints, the well-posedness of the optimal control problem is a difficult matter.

In our numerical examples, we discuss the problem in most of the examples without control constraints. This requires the one-dimensionality of the model. On the other hand, the existence of such wave-type solutions is only meaningful for spatial dimension one.

As standard conclusion of Theorem 2.1, we obtain the following result on the solvability of the optimal control problem:

THEOREM 2.2. *Under the assumptions of Theorem 2.1, the optimal control problem (1.1)–(1.3) has at least one optimal control.*

The result does not depend on the monotonicity of the nonlinearity in the equation and can be proved by exactly the same words as Theorem 5.7 in [31]; notice that the spatial dimension is one. If the box constraints (1.3) are not imposed on f , then we still have existence provided that $\lambda > 0$.

2.2. Adjoint equation and first-order necessary optimality conditions. Assume now that \bar{f} is an optimal or locally optimal control of the problem and let \bar{u} denote the associated state. Then this solution has to obey the standard first-order necessary optimality conditions that are based on the differentiability of the control-to-state mapping $f \mapsto u$. To set them up, we introduce the adjoint equation that is associated to a given pair (f, u) , for instance to (\bar{f}, \bar{u}) :

$$\begin{aligned} -p_t - p_{xx} + R'(u)p &= c_Q(u - u_Q) && \text{in } Q \\ p(x, T) &= c_T(u(x, T) - u_T(x)) && \text{in } \Omega \\ p_x(0, t) = p_x(L, t) &= 0 && \text{in } (0, T). \end{aligned} \tag{2.2}$$

The solution p of this equation is said to be the *adjoint state* associated with the pair (f, u) and denoted below by p_f to indicate the correspondence with f . In the same way, we will denote the state u associated with f by u_f .

The existence and uniqueness of p in $W(0, T)$ is a standard known result, we refer to [31]. Moreover, the following result is known:

THEOREM 2.3 (First-order necessary conditions). *Let $\bar{f} \in L^2(Q)$ be optimal (or locally optimal) for the problem (1.1)–(1.3) and let $\bar{p} := p_{\bar{u}}$ be the associated adjoint state. Then the variational inequality*

$$\int_Q (b(x, t)\bar{p}(x, t) + \lambda\bar{f}(x, t))(f(x, t) - \bar{f}(x, t)) \, dxdt \geq 0 \quad \forall f \in F_{ad} \tag{2.3}$$

must be fulfilled. If $\lambda > 0$, then the projection formula

$$\bar{f}(x, t) = \mathbb{P}_{[f_a, f_b]} \left\{ -\frac{1}{\lambda} b(x, t)\bar{p}(x, t) \right\}$$

has to be satisfied for almost all $(x, t) \in Q$, where $\mathbb{P}_{[f_a, f_b]} : \mathbb{R} \rightarrow \mathbb{R}$ denotes the projection onto the interval $[f_a, f_b]$. For this result, we refer to Casas [5], Raymond and Zidani [27], or to the exposition in [31], Section 5.5.1. The associated proofs can be transferred to the case of the Schlögl model after having transformed the state equation as in the proof of Theorem 1.

By (1.1), the objective functional J is defined that depends on the state u_f and the control f . Since u_f is determined uniquely by f , a mapping $\hat{J} : f \mapsto J(u_f, f)$ is defined, the so-called *reduced objective functional*. The functional $\hat{J} : L^2(Q) \rightarrow \mathbb{R}$ is twice continuously Fréchet differentiable and its derivative is given by

$$\hat{J}'(f)v = \int_Q (b(x, t)p_f(x, t) + \lambda f(x, t))v(x, t) \, dxdt,$$

where p_f is the adjoint state associated with the state u_f by the adjoint equation (2.2). The function $b p_f + \lambda f$ is called *reduced gradient* and can be identified with $\hat{J}'(f)$. In this sense, we have

$$\hat{J}'(f) = b p_f + \lambda f.$$

These facts are well known, we refer e.g. to [31].

2.3. The discretized state and adjoint equation. In the numerical treatment of the optimal control problem, the state equation and the adjoint equation must be discretized. To the state equation, we apply a semi-implicit Euler method with respect to the time and a standard finite element method with piecewise linear and continuous ansatz functions with respect to the space variable. However, the discretization of the adjoint equation (2.2) should be performed with care so that the discretized adjoint equation is the adjoint equation to the discretized state equation.

The discretization of the continuous adjoint equation is not necessarily the adjoint equation of the discretized state equation. This difficulty of potential non-commutativity of the adjoint schemes with respect to discretization is well known. While this fact is often not that important for the optimal control of semilinear equations with monotone nonlinearity, it turned out to be essential for our problems. Using the adjoint equation to the discretized state equation we observed a much faster convergence of the conjugate gradient method than for a straightforward discretization of the continuous adjoint equation.

2.3.1. Numerical solution of the state equation. As we have pointed out, we use piecewise linear and continuous finite elements for the space discretization and a semi-implicit Euler method with respect to the time.

By $\varphi_1, \dots, \varphi_m$ we denote the standard piecewise linear and continuous ansatz functions "hat functions" defined on the interval $[0, L]$ under the equidistant partition

$$0 = x_1 < \dots < x_m = L.$$

For the discretization of u , f , and u_0 with respect to the space variable, we apply the finite element ansatz

$$u(x, t) = \sum_{i=1}^m u^i(t) \varphi_i(x), \quad f(x, t) = \sum_{i=1}^m f^i(t) \varphi_i(x), \quad u_0(x) = \sum_{i=1}^m u_0^i \varphi_i(x)$$

with unknown coefficients u^i, f^i, u_0^i . We write these functions of time in associated m -vector functions,

$$\vec{u}(t) = (u^1(t), \dots, u^m(t))^\top, \quad \vec{f}(t) = (f^1(t), \dots, f^m(t))^\top, \quad \vec{u}_0 = (u_0^1, \dots, u_0^m)^\top.$$

In the sequel, we apply the notation

$$R(\vec{u}) := (R(u^1), \dots, R(u^m))^\top \text{ in particular } \vec{u}^3 = ((u^1)^3, \dots, (u^m)^3)^\top.$$

Multiplying the PDE of the Schlögl model by φ_j for all $j = 1, \dots, m$, we obtain after integration on Ω and an integration by parts in a standard way the system of nonlinear ordinary differential equations

$$\sum_{i=1}^m \left[\dot{u}^i(t) \int_{\Omega} \varphi_i \varphi_j dx + u^i(t) \int_{\Omega} \varphi_i' \varphi_j' dx \right] + \int_{\Omega} R \left(\sum_{i=1}^m u^i(t) \varphi_i \right) \varphi_j dx = \sum_{i=1}^m f^i(t) \int_{\Omega} \varphi_i \varphi_j dx.$$

In the node points x_j associated with φ_j , there holds

$$R\left(\sum_{i=1}^m u^i(t)\varphi_i(x_j)\right) = R\left(\sum_{i=1}^m u^i(t)\delta_{ij}\right) = R(u^j(t)).$$

The function $\tilde{u}(x,t) := \sum_{i=1}^m R(u^i(t))\varphi_i(x)$ is piecewise linear w.r. to x and coincides with the function $R(\sum_{i=1}^m u^i(t)\varphi_i(x))$ in the points x_j . The difference of these two functions is of the order h^2 . Because this is also the order of the finite element discretization error of the equation, we can use the linear approximation $\tilde{u}(x,t)$ as a substitute for $R(\sum_{i=1}^m u^i(t)\varphi_i(x_j))$. This does not decrease the approximation order of our scheme but simplifies the numerical solution considerably. By this simplification, we arrive at the initial value problem

$$M\frac{d}{dt}\vec{u}(t) + K\vec{u}(t) + MR(\vec{u}(t)) = M\vec{f}(t) \quad (2.4)$$

$$\vec{u}(0) = \vec{u}_0. \quad (2.5)$$

Here, M and K denote the mass and stiffness matrices with the entries

$$M_{ij} = \int_{\Omega} \varphi_i \varphi_j dx, \quad K_{ij} = \int_{\Omega} \varphi_i' \varphi_j' dx, \quad i, j = 1, \dots, m.$$

The nonlinear system of ordinary differential equations (2.4) is solved by a semi-implicit Euler method. We split $[0, T]$ by the equidistant partitioning $0 = t_0 \leq t_1 \leq \dots \leq t_n = T$ with time step $\tau = T/n$ and approximate the values $\vec{u}(t_i)$ by vectors \vec{u}_i , $i = 1, \dots, n$, i.e. $\vec{u}(t_i) \sim \vec{u}_i$. Moreover, we discretize f by a vector-valued step function with values \vec{f}_i . This amounts to

$$\frac{1}{\tau}M(\vec{u}_i - \vec{u}_{i-1}) + K\vec{u}_i + MR(\vec{u}_{i-1}) = M\vec{f}_i, \quad i = 1, \dots, n.$$

In the particular case $R(u) = ku^3 - au$, this means

$$\left(\frac{1}{\tau}M + K\right)\vec{u}_i = \frac{1}{\tau}M\vec{u}_{i-1} + M(a\vec{u}_{i-1} - k(\vec{u}_{i-1})^3) + M\vec{f}_i, \quad i = 1, \dots, n.$$

2.3.2. Discretization of the optimal control problem. Analogously to u and f , we discretize u_Q and u_T by

$$u_Q(x,t) = \sum_{i=1}^m u_Q^i(t)\varphi_i(x), \quad u_T(x) = \sum_{i=1}^m u_T^i\varphi_i(x) \quad (2.6)$$

with coefficients $\vec{u}_Q(t) := (u_Q^1(t), \dots, u_Q^m(t))^\top$, $\vec{u}_T := (u_T^1, \dots, u_T^m)^\top$. In the objective functional, integrals with respect to t are approximated by those for step functions, i.e

$$\int_0^T z(t)dt \approx \tau \sum_{i=1}^n z(t_i),$$

where we adopt the points t_i from the time discretization of the state equation. To approximate the objective functional J , we need the values \vec{u}_i and \vec{f}_i , $i = 1, \dots, n$. In view of the discretization of u, u_Q, u_T, f we obtain

$$\begin{aligned}
J(u, f) &= \frac{c_Q}{2} \iint_Q \left(\sum_{i=1}^m (u^i(t) - u_Q^i(t)) \varphi_i(x) \right)^2 dx dt + \frac{c_T}{2} \int_{\Omega} \left(\sum_{i=1}^m (u^i(T) - u_T^i) \varphi_i(x) \right)^2 dx \\
&\quad + \frac{\lambda}{2} \iint_Q \left(\sum_{i=1}^m f^i(t) \varphi_i(x) \right)^2 dx dt \\
&= \frac{c_Q}{2} \int_0^T (\vec{u}(t) - \vec{u}_Q(t))^\top M (\vec{u}(t) - \vec{u}_Q(t)) dt + \frac{c_T}{2} (\vec{u}(T) - \vec{u}_T)^\top M (\vec{u}(T) - \vec{u}_T) \\
&\quad + \frac{\lambda}{2} \int_0^T \vec{f}(t)^\top M \vec{f}(t) dt \sim J_{h,\tau}(\vec{u}_1, \dots, \vec{u}_n, \vec{f}_1, \dots, \vec{f}_n) \\
&:= \tau \sum_{i=1}^n \left[\frac{c_Q}{2} (\vec{u}_i - \vec{u}_Q(t_i))^\top M (\vec{u}_i - \vec{u}_Q(t_i)) + \frac{\lambda}{2} \vec{f}_i^\top M \vec{f}_i \right] + \frac{c_T}{2} (\vec{u}_n - \vec{u}_T)^\top M (\vec{u}_n - \vec{u}_T).
\end{aligned}$$

The discretized optimal control problem reads

$$\min J_{h,\tau}(\vec{u}_1, \dots, \vec{u}_n, \vec{f}_1, \dots, \vec{f}_n) \quad (2.7)$$

subject to

$$\frac{1}{\tau} M (\vec{u}_i - \vec{u}_{i-1}) + K \vec{u}_i + M R (\vec{u}_{i-1}) = M \vec{f}_i, \quad i = 1, \dots, n, \quad (2.8)$$

$$\vec{f}_a \leq \vec{f}_i \leq \vec{f}_b, \quad i = 1, \dots, n. \quad (2.9)$$

where \vec{u}_0 is fixed according to (2.5).

2.3.3. The discrete adjoint equation. Let us derive the adjoint equation to the discretized optimal control problem (2.7)–(2.9). To this aim, we introduce the *discrete Lagrangian* \mathcal{L} that considers ("eliminates") the state equations by Lagrange multipliers \vec{p}_i , $i = 1, \dots, n$,

$$\begin{aligned}
\mathcal{L} &= J_{h,\tau} - \tau \sum_{i=1}^n \left\langle \left(\frac{1}{\tau} M + K \right) \vec{u}_i - \frac{1}{\tau} M \vec{u}_{i-1} + M R (\vec{u}_{i-1}) - M \vec{f}_i, \vec{p}_i \right\rangle_{\mathbb{R}^m} \\
&= J_{h,\tau} - \tau \sum_{i=1}^n \left\langle \left(\frac{1}{\tau} M + K \right) \vec{u}_i - M \vec{f}_i, \vec{p}_i \right\rangle_{\mathbb{R}^m} + \tau \sum_{i=0}^{n-1} \left\langle \frac{1}{\tau} M \vec{u}_i - M R (\vec{u}_i), \vec{p}_{i+1} \right\rangle_{\mathbb{R}^m}, \quad (2.10)
\end{aligned}$$

where $\langle \cdot, \cdot \rangle_{\mathbb{R}^m}$ denotes the inner product of \mathbb{R}^m . It is well known that the discrete adjoint system is composed of the equations $\partial \mathcal{L} / \partial \vec{u}_j = 0$, $j = 1, \dots, n$.

First, we evaluate the equations $\partial \mathcal{L} / \partial \vec{u}_j = 0$ for $j = 1, \dots, n-1$: We obtain for all $\vec{h} \in \mathbb{R}^m$

$$0 = \tau \left[\left\langle c_Q M (\vec{u}_j - \vec{u}_Q(t_j)) - \left(\frac{1}{\tau} M + K \right)^\top \vec{p}_j + \frac{1}{\tau} M^\top \vec{p}_{j+1} - \text{diag}(R'(\vec{u}_j)) M \vec{p}_{j+1}, \vec{h} \right\rangle_{\mathbb{R}^m} \right].$$

By the symmetry of M and K , this implies

$$-\frac{1}{\tau}M(\vec{p}_{j+1} - \vec{p}_j) + K\vec{p}_j + \text{diag}R'(\vec{u}_j)M\vec{p}_{j+1} = c_Q M(\vec{u}_j - \vec{u}_Q(t_j)), \quad j = 1, \dots, n-1. \quad (2.11)$$

In the case $R(u) = k u^3 - a u$, this amounts to

$$-\frac{1}{\tau}M(\vec{p}_{j+1} - \vec{p}_j) + K\vec{p}_j + (3k \text{diag}(\vec{u}_j^2) - aI)M\vec{p}_{j+1} = c_Q M(\vec{u}_j - \vec{u}_Q(t_j)).$$

Analogously, we derive for $j = n$ the equation

$$\left(\frac{1}{\tau}M + K\right)\vec{p}_n = c_Q M(\vec{u}_n - \vec{u}_Q(t_n)) + \frac{c_T}{\tau}M(\vec{u}_n - \vec{u}_T). \quad (2.12)$$

The discrete adjoint system is formed by the equations (2.11)–(2.12). Setting for convenience

$$\vec{p}_{n+1} := c_T(\vec{u}_n - \vec{u}_T),$$

we get an equation analogous to the case $j \in \{1, \dots, n-1\}$, but here the nonlinear term does not appear:

$$-\frac{1}{\tau}M(\vec{p}_{n+1} - \vec{p}_n) + K\vec{p}_n = c_Q M(\vec{u}_n - \vec{u}_Q(t_n)).$$

3. The Schlögl model and wave type solutions. In this section, we explain the existence of traveling waves and their principal behavior. Let us consider the more general version of the Schlögl model

$$u_t = Du_{xx} - k(u - u_1)(u - u_2)(u - u_3). \quad (3.1)$$

with additional constant $D > 0$. This model is one of very few for which traveling wave solutions are known to exist.

3.1. Transformation from the general model to the standard form. Here, we follow the exposition in [23]. The general Schlögl model (3.1) can be transformed to the standard Schlögl model (3.3). First, one performs a change of variables in (3.1), $u(x, t) = \tilde{u}(x, t)(u_3 - u_1) + u_1$, that yields for the reaction term

$$\begin{aligned} R(u) &= k\tilde{u}(u_3 - u_1)(\tilde{u}(u_3 - u_1) - (u_2 - u_1))(\tilde{u}(u_3 - u_1) - (u_3 - u_1)) \\ &= k(u_3 - u_1)^2\tilde{u}(\tilde{u}(u_3 - u_1) - (u_2 - u_1))(\tilde{u} - 1) \\ &= k(u_3 - u_1)^3\tilde{u}\left(\tilde{u} - \frac{(u_2 - u_1)}{(u_3 - u_1)}\right)(\tilde{u} - 1). \end{aligned}$$

After this substitution, the partial differential equation (3.1) admits the form

$$(u_3 - u_1)\frac{\partial\tilde{u}}{\partial t} = (u_3 - u_1)D\frac{\partial^2\tilde{u}}{\partial x^2} - k(u_3 - u_1)^3\tilde{u}\left(\tilde{u} - \frac{(u_2 - u_1)}{(u_3 - u_1)}\right)(\tilde{u} - 1). \quad (3.2)$$

For convenience, we introduce the new parameters

$$\kappa = k(u_3 - u_1)^2, \quad \tilde{u}_2 = \frac{(u_2 - u_1)}{(u_3 - u_1)}.$$

By $u_1 < u_2 < u_3$, we have $0 < \tilde{u}_2 < 1$. Now (3.2) can be written as

$$\frac{1}{\kappa} \tilde{u}_t = \frac{D}{\kappa} \tilde{u}_{xx} - \tilde{u}(\tilde{u} - 1)(\tilde{u} - \tilde{u}_2).$$

Next, we introduce the new coordinates $\tilde{t} = \kappa t$, $\tilde{x} = \sqrt{\kappa/D} x$ and the transformed function $\tilde{u}(\tilde{x}, \tilde{t}) := u(\sqrt{\frac{D}{\kappa}} \tilde{x}, \frac{1}{\kappa} \tilde{t})$. Then an easy computation leads to the transformed partial differential equation in the standard form of the Schlögl model,

$$\frac{\partial}{\partial \tilde{t}} \tilde{u}(\tilde{x}, \tilde{t}) = \frac{\partial^2}{\partial \tilde{x}^2} \tilde{u}(\tilde{x}, \tilde{t}) - \tilde{u}(\tilde{x}, \tilde{t})(\tilde{u}(\tilde{x}, \tilde{t}) - \tilde{u}_2)(\tilde{u}(\tilde{x}, \tilde{t}) - 1). \quad (3.3)$$

In this case, the velocity of the travelling wave front is

$$\tilde{c} = \frac{1}{\sqrt{2}}(1 - 2\tilde{u}_2), \quad (3.4)$$

we refer to formula (3.8) below.

3.2. Traveling wave solutions. The existence of traveling wave fronts is known for the infinite domain $(-\infty, \infty)$ instead of $(0, L)$. However, if L is sufficiently large, then the solution of the Schlögl model behaves similar as a traveling wave front. To motivate the existence of traveling wave fronts, we follow again [23]. We introduce a co-moving coordinate ξ by

$$\xi = x - ct$$

and define a function $z : \mathbb{R} \rightarrow \mathbb{R}$ with $z(x - ct) := u(x, t)$ for all (x, t) that belong to the domain of definition and a suitable constant $c \in \mathbb{R}$ (velocity of the wave front). From the Schlögl model for u , we easily get an ODE for z ,

$$D z''(\xi) + k z'(\xi) + R(z(\xi)) = 0. \quad (3.5)$$

Moreover, we require the boundary conditions

$$\lim_{\xi \rightarrow -\infty} z(\xi) = u_3, \quad \lim_{\xi \rightarrow \infty} z(\xi) = u_1.$$

Solving of (3.5) can be done by the following substitution, see [22],

$$z' = B(z - u_1)(z - u_3) \quad (3.6)$$

which results in

$$0 = (u_1 - z)(z - u_3)(-Bc + B^2(u_1 + u_3) - ku_2 + (k - 2DB^2)z).$$

This can hold, except for $z = u_1$ and $z = u_2$, only if

$$c = \pm \sqrt{\frac{Dk}{2}}(u_1 + u_3 - 2u_2), \quad B = \pm \sqrt{\frac{k}{2D}}.$$

To solve (3.6), we perform again a change of variables, $z(\xi) = \frac{1}{2}(u_3 - u_1)(y(\xi) + 1) + u_1$, that yields a nonlinear differential equation for y ,

$$y' = \frac{1}{2}B(u_3 - u_1)(y^2 - 1).$$

Introducing a new parameter \tilde{B} by $B = 2\tilde{B}/(u_3 - u_1)$ gives

$$\frac{1}{\tilde{B}} \frac{d}{d\xi} y(\xi) = (y^2(\xi) - 1).$$

This equation can be further simplified by the substitutions

$$\tilde{\xi} = \tilde{B}\xi, \quad \tilde{y}(\tilde{B}\xi) = y(\xi)$$

to obtain (the tilde is omitted for convenience)

$$y' = y^2 - 1$$

with boundary conditions

$$\lim_{\xi \rightarrow -\infty} y(\xi) = 1, \quad \lim_{\xi \rightarrow \infty} y(\xi) = -1.$$

This ordinary differential equation can be integrated by separation of variables. With an integration constant c_1 , two possible solutions are obtained,

$$y_1 = -\tanh(\xi + c_1), \quad y_2 = -\coth(\xi + c_1).$$

Obviously, only y_1 is bounded so that y_2 can be excluded from further consideration. The integration constant is obtained by the initial condition and can assumed to be zero because it only corresponds to a phase shift of the (stationary shaped) traveling wave front. Substituting back all changes of coordinates and variables gives

$$y(\xi) = -\tanh(\tilde{B}\xi) = -\tanh\left(\frac{B}{2}\xi(u_3 - u_1)\right).$$

Finally, the traveling wave front of the Schlögl model is found as

$$z(\xi) = U_c(\xi) := \frac{1}{2} \left(u_1 + u_3 + (u_1 - u_3) \tanh \left(\frac{1}{2} \sqrt{\frac{k}{2D}} (u_3 - u_1) \xi \right) \right)$$

with the velocity

$$c = \sqrt{\frac{Dk}{2}} (u_1 + u_3 - 2u_2). \quad (3.7)$$

As we have seen, it is always possible to transform the general Schlögl model to its standard form

$$\frac{\partial u}{\partial t} = \frac{\partial^2 u}{\partial x^2} - u(u - u_2)(u - 1), \quad 0 < u_2 < 1,$$

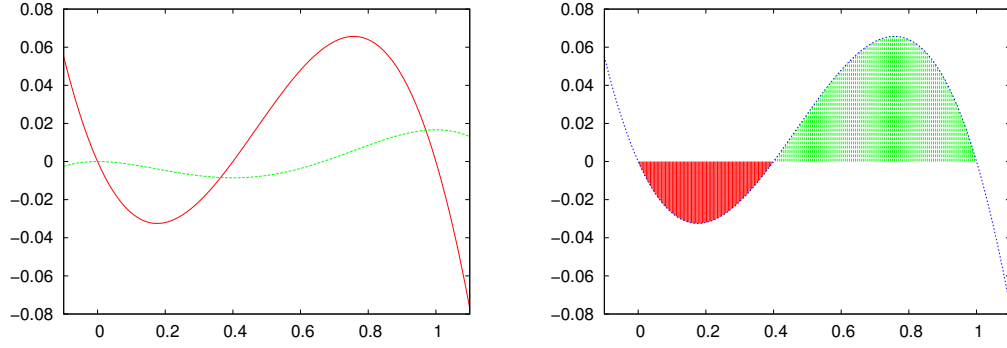


FIG. 3.1. *Left: Reaction term R (solid) and corresponding potential V (dashed) for $u_1 = 0$, $u_2 = 0.4$, $u_3 = 1$, $k = 1$. Right: Reaction term R and areas corresponding to the two integrals in equation (3.9).*

This corresponds to the form above with $D = k = 1$, $u_1 = 0$ and $u_3 = 1$. In this standard form, (3.2) and (3.7) simplify to

$$U_c(\xi) = \frac{1}{2} \left(1 - \tanh \left(\frac{1}{2\sqrt{2}} \xi \right) \right) = \frac{1}{1 + \exp(\frac{\xi}{\sqrt{2}})},$$

$$c = \frac{1}{\sqrt{2}}(1 - 2u_2). \quad (3.8)$$

3.3. A mechanical analog. The Newtonian equation of motion for an object with mass m , friction coefficient ρ , and force F is in the 1D case

$$m x''(t) - \rho x'(t) - F = 0.$$

Compared with (3.5), we have the relations

$$m \sim D, \quad \rho \sim -c, \quad R \sim -F.$$

Therefore, the problem of a traveling wave solution can be considered as the problem of a particle that moves under friction in a potential with given initial and end values. To the reaction term R , there corresponds a potential V . Both functions can be seen in Fig. 3.1. The initial values would be $x(0) = u_3$, $x'(0) = 0$ and the terminal values $x(T) = u_1$, $x'(T) = 0$. In the mechanical analog, these correspond to the maxima of the potential.

A trajectory should be found that starts from the right (global in the picture) maximum of the potential with zero velocity, moves down the potential and reaches the (local in the picture) maximum at the left, where the particle stops. This can only work if the friction dissipates the energy difference between the two maxima. If the two maxima have the same height, the friction must be zero. Due to that correspondence, this means that the velocity of the front in the Schlögl model must be zero if the reaction term R is antisymmetric with respect to some $\alpha \in \mathbb{R}$, i.e. it holds $R(\alpha + u) = -R(\alpha - u)$ and therefore V is symmetric, i.e. $V(\alpha + u) = V(\alpha - u)$.

Because V is the primitive of R , the case of equal height of the maxima u_1, u_2 of V can be interpreted in another way.

$$V(u_3) - V(u_1) = \int_0^{u_3} R(u) du - \int_{u_1}^0 R(u) du = \int_{u_2}^{u_3} R(u) du - \int_{u_1}^{u_2} R(u) du. \quad (3.9)$$

If the value of the potential at the maxima is the same, $V(u_3) - V(u_1) = 0$, then the two integrals are equal. This means that the red area (below $u = 0$ and above $R(u)$) and the green area (above $u = 0$ and below $R(u)$) in Fig. 3.1 must be equal. This happens e.g. in the case $u_1 = -u_3, u_2 = 0$. Then the speed of a front, which connects the two stable fixpoints of $R(u)$, will be zero, and hence the wave front will not move.

4. Proper Orthogonal Decomposition (POD).

4.1. Short description of POD. For nonlinear partial differential equations, proper orthogonal decomposition (POD) is one of the widely used methods of model reduction. This technique, also known as Karhunen-Loeve decomposition, determines low dimensional subspaces, where the main behavior of the solution to the original state equation is still reflected in a high or at least acceptable precision.

In this paper, we apply the method of snapshots. For some fixed control function $f := f_{\text{snap}}$, we determine the solution u of the state equation (1.2) at the time instances $0 = t_0 < t_1 < \dots < t_n = T$ that were already used for the time discretization of (1.2). The so-called snapshots $u_0^s = u(t_0), \dots, u_n^s = u(t_n)$ form a high-dimensional subspace of $H^1(0, L)$ of finite dimension.

By POD, for given natural number $r \geq 1$, linear combinations ψ_1, \dots, ψ_r of the snapshots u_0^s, \dots, u_n^s are determined, which solve the following quadratic optimization problem in the space $H = L^2(0, L)$:

$$\begin{aligned} \min_{v_1, \dots, v_r \in H} \quad & \sum_{i=0}^n \alpha_i \left\| u_i^s - \sum_{j=1}^r (u_i^s, v_j)_H v_j \right\|_H^2 \\ \text{subject to} \quad & (v_i, v_j)_H = \delta_{ij} \quad \forall i, j \in \{1, \dots, r\}, \end{aligned}$$

with given trapezoidal weights $\alpha_0, \dots, \alpha_n$. The solution of this optimization problem is determined by a singular value decomposition. We do not explain these details and refer the reader to Kunisch and Volkwein [16], Volkwein [32], Fahl and Sachs [9] or Arian et al. [2] and the references therein.

The functions ψ_1, \dots, ψ_r form the so-called POD basis. The solution u of (1.2) is approximated in the r -dimensional subspace $\text{span}\{\psi_1, \dots, \psi_r\}$. Instead of the finite element approximation, now the ansatz

$$u(x, t) = \sum_{i=1}^r U^i(t) \psi_i(x)$$

is applied in the standard Ritz Galerkin method. In what follows, we shall denote the solutions of POD reduced problems by capital letters. The POD basis functions ψ_1, \dots, ψ_r were obtained by the finite element method, hence they are linear combinations of the FE ansatz functions $\varphi_1, \dots, \varphi_m$,

$$\psi_i(x) = \sum_{k=1}^m \psi_k^i \varphi_k(x), \quad i = 1, \dots, r.$$

We collect the coefficients by column vectors $\vec{\psi}_i = (\psi_1^i, \dots, \psi_k^i)^\top \in \mathbb{R}^m$ and define the matrix $\Psi := (\vec{\psi}_1 | \dots | \vec{\psi}_r)$. The control f and the initial data u_0 are discretized as in (2.6) by the finite element basis functions. After quite a number of calculations, we arrive at the following reduced state equation:

$$\begin{aligned} M^p \frac{d}{dt} \vec{U}(t) + K^p \vec{U}(t) - a M^p \vec{U}(t) + k \Psi^\top M (\Psi \vec{U}(t))^3 &= \Psi^\top M \vec{f}(t) \\ M^p u(0) &= \Psi^\top M \vec{u}_0, \end{aligned} \quad (4.1)$$

where M is the mass matrix introduced in Section 2.3.1 and M^p , K^p are the mass and stiffness matrices for the POD based Galerkin method,

$$\begin{aligned} M_{ij}^p &= (\psi_i, \psi_j)_{L^2(\Omega)}, \quad i, j \in \{1, \dots, r\} \\ K_{ij}^p &= (\dot{\psi}_i, \dot{\psi}_j)_{L^2(\Omega)}, \quad i, j \in \{1, \dots, r\} \\ M_{ij} &= (\varphi_i, \varphi_j)_{L^2(\Omega)}, \quad i, j \in \{1, \dots, m\}. \end{aligned}$$

Notice that, for $t \in [0, T]$, we have $\vec{U}(t) \in \mathbb{R}^r$, while it holds $\vec{f}(t) \in \mathbb{R}^m$. The reduced system (4.1) is solved, analogously to (2.8), by the semi-implicit Euler method.

4.2. Numerical treatment of the adjoint equation by POD. After a couple of transformations, the objective functional of the reduced system is obtained as follows:

$$\begin{aligned} J &= \frac{c_Q}{2} \iint_Q \left(\sum_{l=1}^r U^l(t) \psi_l(x) - \sum_{j=1}^m u_Q^j(t) \varphi_j(x) \right)^2 dx dt \\ &+ \frac{c_T}{2} \int_{\Omega} \left(\sum_{l=1}^r U^l(T) \psi_l(x) - \sum_{j=1}^m u_T^j \varphi_j(x) \right)^2 dx + \frac{\lambda}{2} \iint_Q \left(\sum_{j=1}^m f^j(t) \varphi_j(x) \right)^2 dx dt \\ &\sim \tau \sum_{i=1}^n \left[\frac{c_Q}{2} \left(\Psi \vec{U}_i - (\vec{u}_Q)_i \right)^\top M \left(\Psi \vec{U}_i - (\vec{u}_Q)_i \right) + \frac{\lambda}{2} \vec{f}_i^\top M \vec{f}_i \right] \\ &+ \frac{c_T}{2} \left(\Psi \vec{U}_n - \vec{u}_T \right)^\top M \left(\Psi \vec{U}_n - \vec{u}_T \right). \end{aligned}$$

There are two principal options for establishing the reduced adjoint equation. The first is to derive the one that is associated with the discretized reduced optimal control problem that was based on the snapshots for the state equation. In this way, the exact gradient of the reduced and discretized objective functional is obtained. While this is of importance for the performance of descent methods, it might lead to an unsatisfactory approximation of the exact adjoint state that is associated with the given state function. The POD basis computed for the state function will not in general be suitable for the adjoint state.

We observed this in our computations and worked also with a different POD basis for the adjoint state. In the application to the nonlinear cg method, we preferred to use the first version, since that improved its performance. Therefore, we do not report on our results with the second option that enabled us to compute very good POD approximations of the true adjoint state.

To invoke the first option, we consider the Lagrangian \mathcal{L} of the reduced model depending on

$(\vec{U}_1, \dots, \vec{U}_n, \vec{f}_1, \dots, \vec{f}_n, \vec{P}_1, \dots, \vec{P}_n)$ that reads

$$\begin{aligned} \mathcal{L} &= J - \tau \sum_{i=1}^n \left\langle \left(\frac{1}{\tau} M^p + K^p \right) \vec{U}_i - \left(\frac{1}{\tau} + a \right) M^p \vec{U}_{i-1} + k \Psi^\top M (\Psi \vec{U}_{i-1})^3 - \Psi^\top M \vec{f}_i, \vec{P}_i \right\rangle_{\mathbb{R}^r} \\ &= J - \tau \sum_{i=1}^n \left\langle \left(\frac{1}{\tau} M^p + K^p \right) \vec{U}_i - \Psi^\top M \vec{f}_i, \vec{P}_i \right\rangle_{\mathbb{R}^r} \\ &\quad + \tau \sum_{i=0}^{n-1} \left\langle \left(\frac{1}{\tau} + a \right) M^p \vec{U}_i - k \Psi^\top M (\Psi \vec{U}_i)^3, \vec{P}_{i+1} \right\rangle_{\mathbb{R}^r}. \end{aligned}$$

Deriving the Lagrangian with respect to the state leads to the following reduced and discrete adjoint system: For $j = 1, \dots, n-1$ we derive with respect to the component \vec{U}_j and find

$$\left(\frac{1}{\tau} M^p + K^p \right) \vec{P}_j - \left(\frac{1}{\tau} + a \right) M^p \vec{P}_{j+1} + 3k \Psi^\top \text{diag}((\Psi \vec{U}_j)^2) M \Psi \vec{P}_{j+1} = c_Q (M^p \vec{U}_j - \Psi^\top M(\vec{u}_Q)_j).$$

For $j = n$, we obtain

$$\left(\frac{1}{\tau} M^p + K^p \right) \vec{P}_n = c_Q (M^p \vec{U}_n - \Psi^\top M(\vec{u}_Q)_n) + \frac{c_T}{\tau} (M^p \vec{U}_n - \Psi^\top M \vec{u}_T).$$

4.3. Numerical tests for selected particular cases. In the context of optimal control problems, we will report on some computational experience with POD for wave type solutions. In general, we observed that the number of POD basis functions must be chosen fairly large. Let us first sketch exemplarily the following problem:

We fix the data $L = 20, T = 10, m = 301, \tau = 1/60, k = 1/3, a = 1, \lambda = 10^{-6}$.

Moreover, we apply the control $f \equiv 0$ and use the same control $f_{snap} \equiv 0$ for computing the snapshots. To have a meaningful adjoint equation, we also need the objective functional. We take $c_Q = 1, c_T = 0, u_T = 0$. Further, we define

$$\begin{aligned} u_0(x) &= \begin{cases} -1.2\sqrt{3}, & x \in [0, 2] \\ 0, & \text{else,} \end{cases} & u_0^Q(x) &= \begin{cases} 1.2\sqrt{3}, & x \in [0, 2] \\ 0, & \text{else,} \end{cases} \\ u_Q &= u(f, u_0^Q) \quad (\text{Schl\"ogl solution for } f \equiv 0 \text{ and } u_0 = u_0^Q). \end{aligned}$$

It is worth mentioning that this non-positive initial function u_0 generates a propagating wave front that links the unstable fixed point 0 with the stable fixed point $-\sqrt{3}$. In contrast to this, the initial function (5.1) does not lead to a travelling front.

The initial function and the associated state, computed by the full FEM model, are shown in Fig. 4.1. Here and in all Figures presenting wave fronts, the vertical axis displays the time while the horizontal one displays the spatial variable.

The state function u^r computed by the reduced POD model does not essentially differ from the FE solution u . Using a separate POD basis for the adjoint equation, we also obtained a very good approximation of the full adjoint state p by the reduced one. We observed that, in contrast to standard parabolic equations with monotone nonlinearity, the POD modes decay fairly slow, cf. Fig. 4.2. Therefore, a larger number of basis functions was needed for an acceptable precision.

We also tested the POD method with discrete empirical interpolation (POD-DEIM) by Chatrantabut and Sorensen, [7]. However, this method did not essentially improve our results. Notice

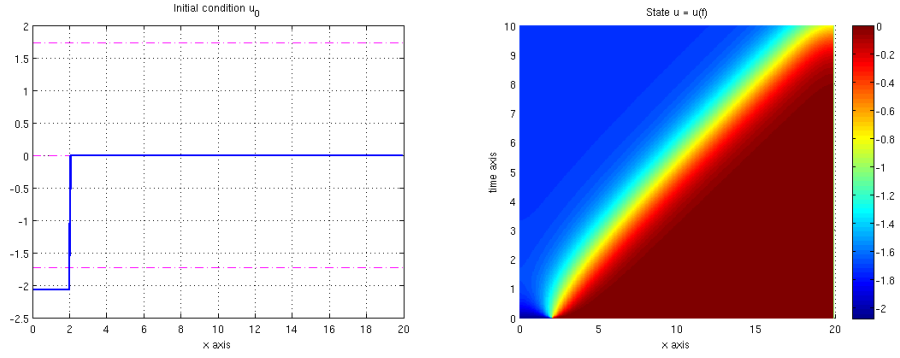


FIG. 4.1. Left: Initial function u_0 , Right: FE solution u of the Schlögl model for $f \equiv 0$.

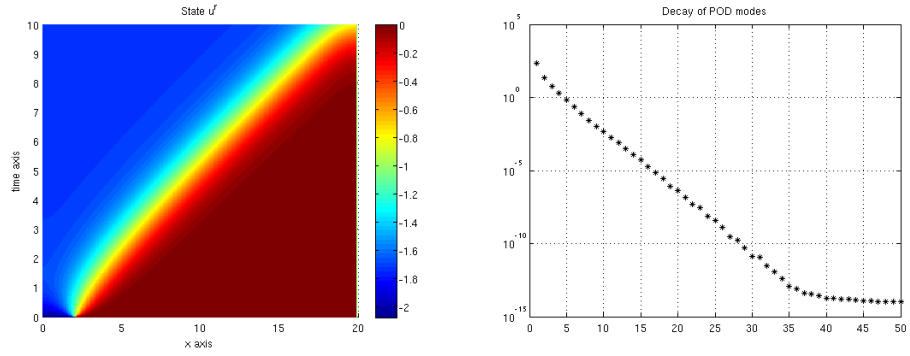


FIG. 4.2. Left: POD solution u^r of the reduced Schlögl model for $f \equiv 0$ with $r = 50$ POD-Basis functions. Right: Decay of the POD modes for u .

that we have already used an interpolation by the special method applied to the nonlinearity,

$$\left(\sum_{i=1}^m u_i \varphi_i \right)^3 \sim \sum_{i=1}^m u_i (\varphi_i)^3.$$

5. Numerical computation of optimal wave fronts. In this section, we discuss several examples of optimal control problems that fit into the following one:

$$\begin{aligned} \min J(u, f) &:= \frac{c_Q}{2} \iint_Q (u(x, t) - u_Q(x, t))^2 dx dt + \frac{c_T}{2} \int_{\Omega} (u(x, T) - u_T(x))^2 dx \\ &+ \frac{\lambda}{2} \iint_Q f^2(x, t) dx dt \end{aligned}$$

subject to

$$\begin{aligned} u_t(x,t) - u_{xx}(x,t) + \frac{1}{3}u^3(x,t) - u(x,t) &= f(x,t) && \text{in } Q \\ u(x,0) &= u_0(x) && \text{in } \Omega \\ u_x(0,t) = u_x(L,t) &= 0 && \text{in } (0,T) \end{aligned}$$

and possibly to the box constraints

$$f_a \leq f(x,t) \leq f_b \quad \text{for a.a. } t \in Q.$$

We shall specify the given data later in the associated examples.

5.1. The nonlinear conjugate gradient method. In our numerical computations, the standard gradient method turned out to be very slow. It took too long time to reach an acceptable precision. This might be explained by the presence of an unstable steady state. Therefore, we applied the nonlinear conjugate method that was much faster and fairly stable.

For convenience, we briefly sketch the different variants of this method, since we observed essential differences in their performance. For a detailed survey on this method, we refer to Hager, [10] and also to Herzog and Kunisch [13], who report on the application of this method in the optimal control of PDEs. Let us first recall the Algorithm, where $u(f)$ and $p(u)$ denote the state u associated with the control f and the adjoint state p associated with the state u , respectively.

Nonlinear conjugate gradient method.

1. *Initialization:* Select an initial control f^0 and an initial step size s_0 . Compute $u^0 = u(f^0)$ (initial state) $p^0 = p(u^0)$ (adjoint state), $g_0 = \lambda f^0 + p^0$ (gradient), $d_0 = -g_0$ (antigradient); set $k := 0$.
2. *New gradient:*

$$\begin{aligned} f^{k+1} &= f^k + s_k d_k && \text{(new control)} \\ u^{k+1} &= u(f^{k+1}) && \text{(new state)} \\ p^{k+1} &= p(u^{k+1}) && \text{(new adjoint state)} \\ g_{k+1} &= \lambda f^{k+1} + p^{k+1} && \text{(new gradient)}. \end{aligned}$$

3. *Direction of descent:* Compute β_{k+1} by g_{k+1}, g_k, d_k according to one of the update formulas below;

$$d^{k+1} = -g_{k+1} + \beta_{k+1} d_k.$$

4. STOP IF $\|g_{k+1}\| < \epsilon$.
5. Select the stepsize s_{k+1} by one of the methods discussed below, $k := k + 1$, GO TO 3.

Update rules for conjugate directions. We used the following known options for defining conjugate directions, cf. [10]:

$$\begin{aligned} \text{Hestenes-Stiefel: } \beta_k &= \frac{g_k^\top (g_k - g_{k-1})}{d_{k-1}^\top (g_k - g_{k-1})}, & \text{Fletcher-Reeves: } \beta_k &= \frac{\|g_k\|^2}{\|g_{k-1}\|^2}, \\ \text{Polak-Ribiere: } \beta_k &= \frac{g_k^\top (g_k - g_{k-1})}{\|g_{k-1}\|^2}, & \text{Hager-Zhang: } \beta_k &= \max(\bar{\beta}_k, \eta_k), \end{aligned}$$

where

$$\eta = 0.01, \quad \gamma = g_k - g_{k-1}, \quad \bar{\beta}_k = \left(\gamma - 2 \frac{\|\gamma\|^2}{d_{k-1}^\top \gamma} d_{k-1} \right)^\top \frac{g_k}{d_{k-1}^\top \gamma}, \quad \eta_k = -\frac{1}{\|d_{k-1}\|} \min(\eta, \|g_{k-1}\|).$$

Step size rules. Among the many standard options for updating the step size, we applied

- *Bisection:* Start by $s_0 > 0$, $k = 0$; Compute $f^{k+1} = f^k + s_k d_k$. If

$$J(u^k, f^k) \leq J(u^{k+1}, f^{k+1})$$

then accept the stepsize. Otherwise repeat the process by $s_k = s_k/2$.

- *Strong Wolfe-Powell rule:* It is required that

$$(i) \quad J(u^{k+1}, f^{k+1}) \leq J(u^k, f^k) + \sigma s_k g_k^\top d_k$$

$$(ii) \quad |g_{k+1}^\top d_k| \leq -\rho g_k^\top d_k$$

We iterate s_k until u^{k+1}, f^{k+1} satisfies (i) and (ii).

- *Step size by Hager and Zhang with guaranteed descent:* The reader is referred to [11].

Next, we discuss the numerical solution of several types of optimal control problems.

5.2. Acceleration of a wave front. We consider first a setting, where – without action of a control – a wave front moves in a constant direction with constant speed. Here, we want to determine a control that changes speed and direction of the wave front in a desired way. To this aim, we solve the optimal control problem for the nonlinearity $R(u) := \frac{1}{3}u^3 - u$. Moreover, let u_{nat} denote the solution of the Schlögl model (1.2) obtained for $f \equiv 0$ and $u_{\text{nat}}(\cdot, 0) = u_0$, where the initial function u_0 is defined by the nonnegative function

$$u_0(x) = \begin{cases} -1.2\sqrt{3}, & x \in [8, 12] \\ 0, & \text{else.} \end{cases}$$

We select the target function

$$u_Q(x, t) = \begin{cases} u_{\text{nat}}(x, t), & t \in [0, 2.5] \\ u_{\text{nat}}(x + ct, 2.5), & \text{else,} \end{cases}$$

where c denotes the velocity of the wave front of u_{nat} in $t = 2.5$. Further, to be closer to practical needs, we restrict the controls to act only close to the boundary of $(0, L)$. We assume that the control only acts in the set $[0, \delta] \cup [L - \delta, L]$ such that $2\delta/L = q < 1$. Let us call this setting *q-sparse control*. This notion differs from that of *sparse controls* in current research. (The support of sparse controls is not fixed in advance and obtained by the optimization process.) The numerical results for $q = 0.9$ and $q = 0.6$ are presented in Fig. 5.1 and Fig. 5.2, respectively.

We obtained the following optimal values of the objective functional J : $J(\bar{u}, \bar{f}) = 0.031129$ for the 0.9-sparse control and $J(\bar{u}, \bar{f}) = 1.1486$ in the 0.6-sparse case. For the regularization parameter, we selected $\lambda = 10^{-6}$. The computations show that acceptable results can also be achieved by sparse controls that act only in certain parts of the domain.

5.3. Steering a wave front to zero. Next, we consider the problem to find a control that steers a traveling wave front, starting from u_0 to one of the three fixed points at the final time $t = T$. This is a fairly trivial task if the fixed point is stable and if no box constraints are imposed on the control. Therefore we concentrate here on the instable fixed point u_2 . We consider again

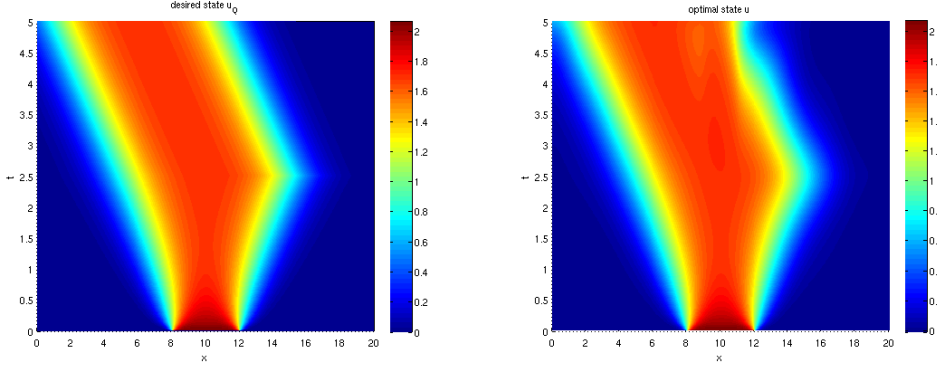


FIG. 5.1. Acceleration of a wave front, 0.9 sparse control; Desired state (left) and optimal state (right).

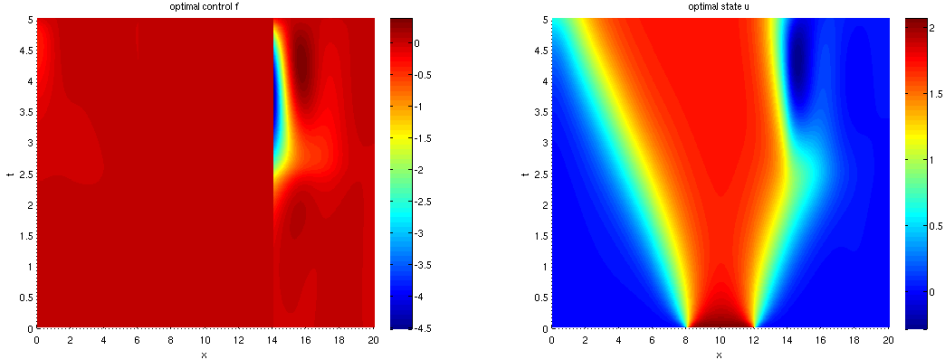


FIG. 5.2. Acceleration of a wave front, 0.6 sparse control; Optimal control (left) and optimal state (right).

the function $R(u) = \frac{1}{3}u^3 - u$, where $u_2 = 0$ is the unstable fixed point, i.e. we want to reach the zero function $u(x,T) = 0$ at the final time T .

Although zero is an unstable fixed point, the optimization process did not cause serious problems. For the objective function we will consider two cases. The first is $c_Q = 0$ and $c_T = 1$; in the second we take $c_Q = 1$ and $c_T = 0$. We select the following initial function:

$$u_0(x) = \begin{cases} -1.2\sqrt{3}, & x \in [0,10) \\ 0, & x = 10 \\ 1.2\sqrt{3}, & x \in (10,20]. \end{cases} \quad (5.1)$$

In view of formula (3.7), here the speed of the wave front is zero without forcing. After a short period of equilibration, the wave stops as it can be observed in Fig. 5.4.

Control in the whole domain. For $c_Q = 0$ and $c_T = 1$, our aim is to reach the zero state at the final time $t = T$. Figure 5.3 displays the result. The optimal objective function value is $J(\bar{u}, \bar{f}) = 4.1916 \cdot 10^{-5}$. The main contribution to this value is due to the control. The deviation to the target state contributes less than one percent.

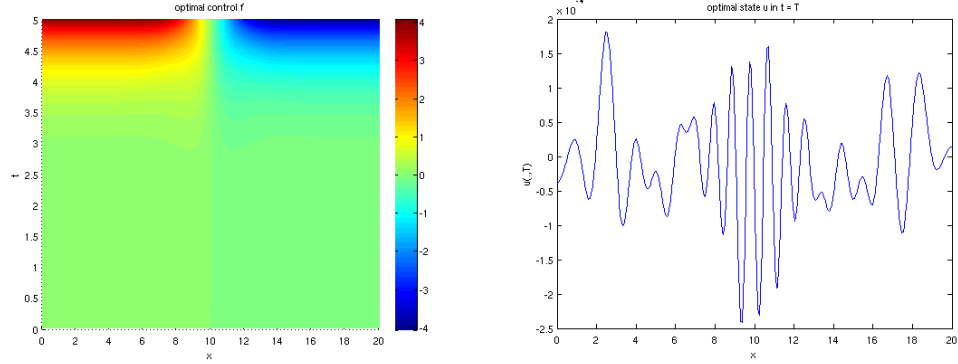


FIG. 5.3. Control to zero in the whole domain; $c_T = 1$. Optimal Control (left) and optimal state (right).

In the second case, our desired state is the function that equals the natural solution u_{nat} till $t = 2.5$, and vanishes after this time. We select $c_T = 0$ and $c_Q = 1$. The optimal value is $J(\bar{u}, \bar{f}) = 0.24576$. Here, the main contribution to this value is due to the difference of the optimal state to the desired state. This is not surprising, since the desired state is obviously not reachable. The result is shown in Fig. 5.4, right-hand side.

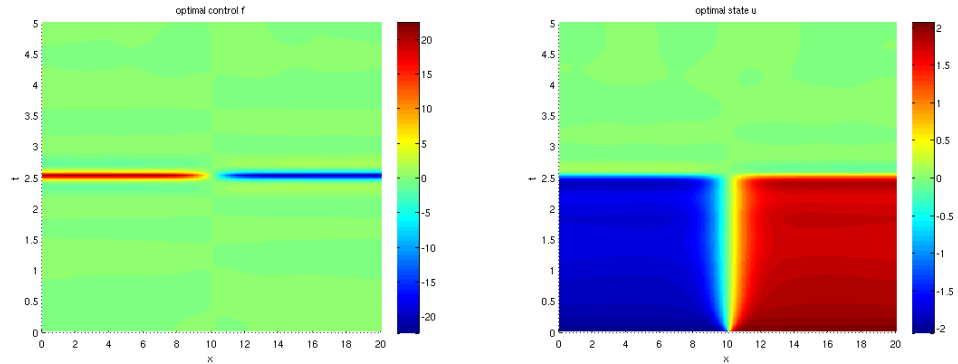


FIG. 5.4. Control to zero in the whole domain; $c_Q = 1$. Optimal Control (left) and optimal state (right).

Sparse controls. Here, the aim is to control of a wave front to the zero state at the final time for the same data as above. We discuss here some other cases for the q -sparse setting. The closer q is to one, the better is the obtained result.

What happens can be seen in Fig. 5.5 which shows the optimal control and the corresponding state at $t = T$ for a 0.7-sparse control. The optimal value $J(\bar{u}, \bar{f}) = 2.3324 \cdot 10^{-2}$ is more than two magnitudes larger than that for a control acting in the whole domain $(0, L)$.

Also an increase in the control amplitude is observed. Compared to the control in the whole domain $(0, L)$, it is approximately three times larger than in the case without spatial restrictions. In the example of extinguishing a wave for $t > 2.5$, this increase in the control amplitude can be observed for values $q \leq 0.7$. For the 0.7-sparse control this is shown in Fig. 5.6.

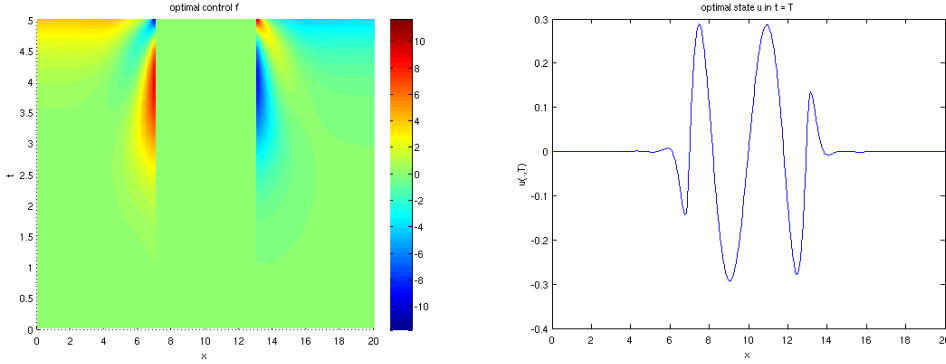


FIG. 5.5. Control to zero by 0.7-sparse control, $c_T = 1$. Optimal control (left), optimal final state (right).

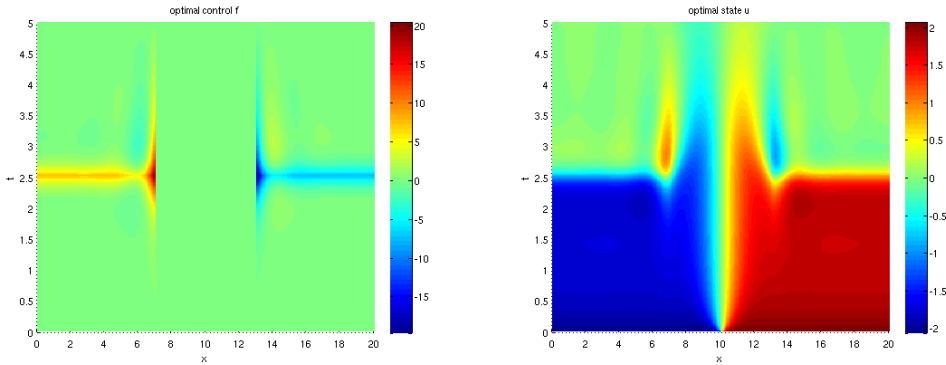


FIG. 5.6. Control to zero by 0.7-sparse control, case $c_Q = 1$; zero target after $t = 2.5$. Optimal control (left) and optimal state (right).

The optimal objective value increases, we have $J(\bar{u}, \bar{f}) = 3.3029$ for the displayed 0.7-sparse control.

Box constraints on the control. We return to the case where the control is allowed to act in the complete domain $(0, L)$, but we add box constraints. We imposed the box constraints $|f(x, t)| \leq 3$ on u and obtained the solutions displayed in Figure 5.7.

To solve this example, we applied a type of projected gradient method that slightly differs from the standard one. For the antigradient as descent direction, we selected the step size without considering the box constraints even if the obtained new (auxiliary) control is unfeasible. Hereafter, this auxiliary control was projected on the admissible set.

The computed optimal value was $J(\bar{u}, \bar{f}) = 4.0009 \cdot 10^{-5}$. To our surprise, this value is smaller than the one obtained for the unrestricted case. This behaviour was also confirmed for smaller bounds of the form $|f(x, t)| \leq b$: For $b = 2.5$, we computed $J(\bar{u}, \bar{f}) = 3.6523 \cdot 10^{-5}$, $b = 2$ delivered $J(\bar{u}, \bar{f}) = 3.2742 \cdot 10^{-5}$, for $b = 1.5$ we found $J(\bar{u}, \bar{f}) = 2.8994 \cdot 10^{-5}$ and $b = 1$ finally brought an increase to $J(\bar{u}, \bar{f}) = 3.777 \cdot 10^{-5}$.

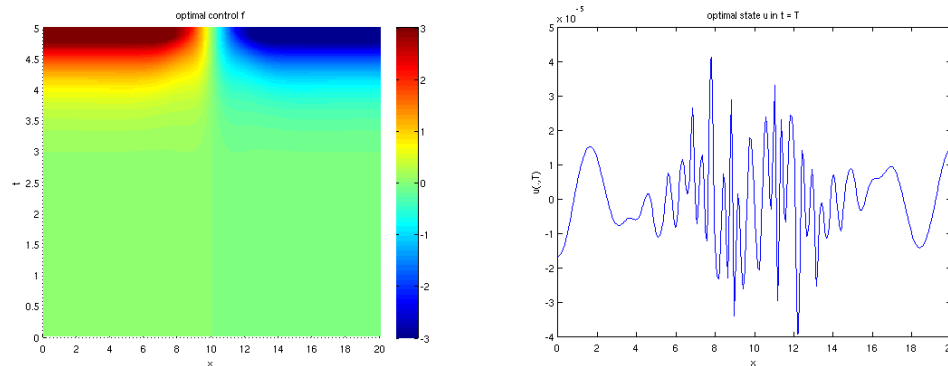


FIG. 5.7. Control to zero at $t = T$ subject to box constraints. Optimal Control (left) and optimal state (right).

This behaviour might be explained by numerical instabilities or by the presence of different local minima that are avoided by the restricted paths of iteration.

5.4. Stopping of a nucleation process.

The stopping problem and a simple direct solution. In the uncontrolled case $f \equiv 0$, the initial function and data below generate a wave front that propagates with constant speed in both spatial directions. This can be interpreted as some kind of nucleation process. We select

$$L = 20, T = 5, k = \frac{1}{3}, a = 1,$$

$$u_0(x) = \begin{cases} 1.2\sqrt{3}, & x \in [9, 11] \\ 0, & \text{else.} \end{cases}$$

This initial function is presented in the left hand side of Fig. 5.8. Solving the Schlögl model with control function $f = 0$, the traveling wave front u_{nat} in Fig. 5.8 (right) is obtained. Notice that the vertical axis displays the time, while the horizontal one shows the space variable. The computations were performed with $m = 300$ and $\tau = 1/80$. Let us denote this uncontrolled traveling wave front by u_{nat} .

The aim is to stop this wave at $t = 2.5$. After stopping, the wave should be kept fixed. To stop the wave front at this time, we will solve the optimal control problem with $c_Q = 1, c_T = 0, \lambda := 10^{-6}, u_T(x) \equiv 0$ to approach the desired trajectory

$$u_Q(x, t) = \begin{cases} u_{\text{nat}}(x, t), & t \in [0, 2.5] \\ u_{\text{nat}}(x, 2.5), & t \in (2.5, T]. \end{cases}$$

We will show below that this optimization method yields reasonable results.

However, in the simpler case without the box constraints (1.3), the following observation leads to a very simple control law that instantly stops the wave at $t = 2.5$: In the interval $[0, 2.5)$ we do nothing, i.e. we follow the uncontrolled solution u_{nat} . At $t = 2.5$, the wave should stop, hence $u_t(x, t) = 0$ must hold. This yields the equation

$$0 = u_{xx}(x, t) - k u(x, t)^3 + u(x, t) + f(x, t).$$

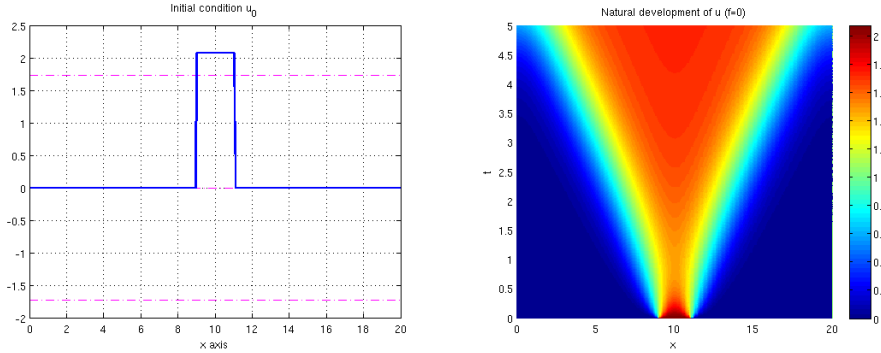


FIG. 5.8. Nucleation process. Initial function u_0 (left) and uncontrolled propagating wave front u_{nat} (right).

Resolving for f , we obtain the control

$$f_{\text{stop}}(x,t) = \begin{cases} 0 & \text{for } t \leq 2.5, \\ k u_{\text{nat}}^3(x,2.5) - u_{\text{nat}}(x,2.5) - \frac{\partial^2}{\partial x^2} u_{\text{nat}}(x,2.5) & \text{for } t > 2.5. \end{cases} \quad (5.2)$$

This argument that was told to us by P. Paulau (TU Berlin, Institute of Theoretical Physics), is mathematically not yet justified, since we did not yet prove that $\frac{\partial^2}{\partial x^2} u_{\text{nat}}(x,2.5)$ is well defined. We will verify this by Theorem 5.1 below. Numerically, we see that this control stops the wave indeed. The control f_{stop} and the associated wave front are shown in Fig. 5.9.

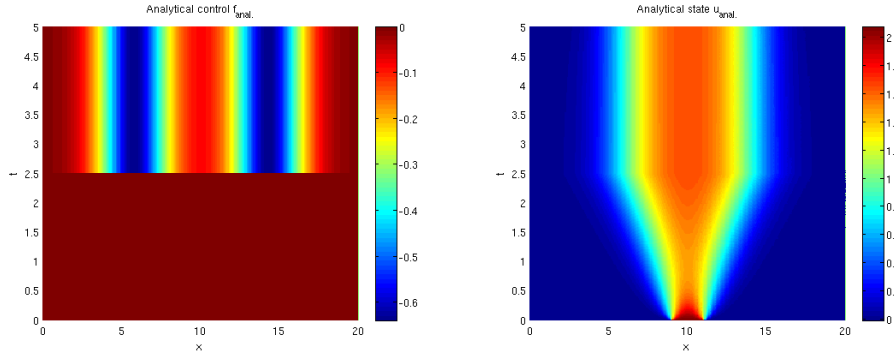


FIG. 5.9. Control f_{stop} and state u_{stop} .

The objective value for this control is not very close to zero, because we also have the contribution of the regularization term for f ; the computed optimal value is

$$J(u_{\text{stop}}, f_{\text{stop}}) = 3.4814 \cdot 10^{-6}.$$

In principle, the same control function is obtained by the optimal control method. However, it was very helpful, if a multiple of f_{stop} was taken as initial control for the nonlinear conjugate gradient method.

It remains to justify the direct stopping method using f_{stop} .

THEOREM 5.1. *Let $u_0 \in L^\infty(0,L)$ be a given initial function and assume that $f = 0$. Then the solution u of (1.2) exhibits the regularity $u \in C((0,T], H^2(0,L))$. Therefore, for all $t \in (0,T]$, there holds $u(\cdot, t) \in H^2(0,L)$.*

Proof. By Theorem 2.1 we already know that u is bounded, i.e. $u \in L^\infty(Q)$. Now Theorem 4 by Di Benedetto [8] can be applied that ensures Hölder continuity of bounded solutions to parabolic equations. By this theorem, we obtain $u \in C^{0,\alpha}([\varepsilon, T], C^{0,\alpha}[0, L])$ for arbitrarily small $\varepsilon > 0$ and some Hölder constant $\alpha \in (0, 1)$ that may depend on ε . In view of this, the function $F : (x, t) \mapsto R(u(x, t))$ is also Hölder continuous on $[\varepsilon, T] \times [0, L]$ with some constant $\tilde{\alpha} \in (0, 1)$. Considering u on the interval $[t_0, T]$ with $t_0 := \varepsilon$ and starting with $u_\varepsilon := u(\cdot, t_0) \in C[0, L] \subset L^2(0, L)$, we have

$$u_t(x, t) - u_{xx}(x, t) = -F(x, t), \quad t \geq t_0,$$

where the right-hand side F belongs to $C^{0,\tilde{\alpha}}([t_0, T], C^{0,\tilde{\alpha}}[0, L]) \subset C^{0,\tilde{\alpha}}([t_0, T], L^2(0, L))$. Now we are able to apply Theorem 1.2.1 in Amann [1] that uses the differential operator $A = -\partial_{xx}$ with domain $D(A) = \{u \in H^2(0, L) : u_x(0) = u_x(L) = 0\}$ and spaces $E_0 = L^2(0, L)$, $E_1 = H^2(0, L)$.

This theorem ensures that the solution u belongs to $C((t_0, T], H^2(0, L))$. Therefore, we have $u(t) \in H^2(0, L)$ for all $t \geq t_0 + \varepsilon = 2\varepsilon$. Since ε can be taken arbitrarily small, the claimed result follows immediately. \square

Stopping by optimal control. Let us now deal with the stopping problem by the optimal control method. Notice that this would be the only option, if the box constraints (1.3) must be imposed. Then the explicitly given function f_{stop} of (5.2) might exceed the prescribed bounds. This can be important in particular for sparse controls because they will attend larger values.

As initial control for the nonlinear cg method, we take first $f^0 = 0.99 f_{\text{stop}}$.

Test 1; FEM – initial control $0.99 f_{\text{stop}}$. We should expect that, by this very good initial control, the cg method will converge quite fast to the solution. However, this was not the case, yet we observed a fairly slow convergence. All computations were stopped after at most 200 iterations of the cg method. We tested all variants of the nonlinear cg method and of stepsize rules surveyed in Section 5.1 and obtained diverse results. We did not figure out a method that is superior over the others, since different methods were the best with respect to the final precision, the computing time, or with respect to the iteration number. Moreover, this varied in the different examples. Therefore, the following tables are not representative for the optimization runs with different data. However, on average, the displayed combinations belonged to the best with respect to all criteria. They were obtained with the step size rule suggested by Hager and Zhang.

Method	Hestenes-Stiefel	Fletcher-Reeves	Polak-Ribiere	Hager-Zhang
Optimal objective value	3.9041e-06	3.004e-06	2.9895e-06	3.0573e-06
CPU time (in s)	100.03	78.3	86.69	101.87

TABLE 5.1
Test 1, Optimal objective and CPU times for optimizing the FE model.

Graphically, the optimal control is very close to the "exact stopping control" f_{stop} , cf. Fig. 5.10. There is only a tiny deviation of the computed optimal control f from f_{stop} . Though marginal,

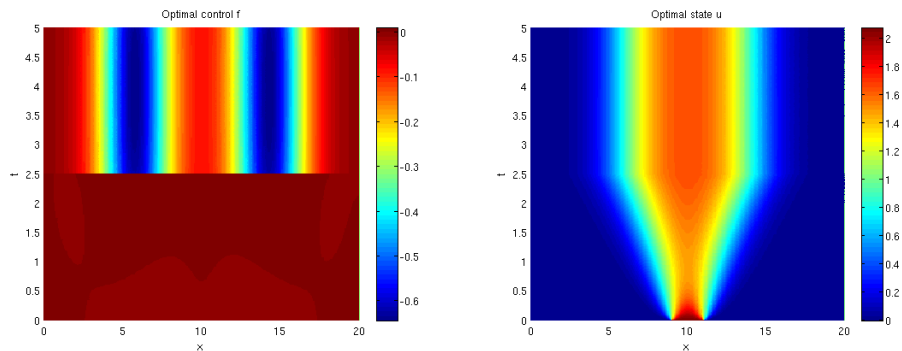


FIG. 5.10. *Test 1, Optimal control (left) and optimal state (right).*

this slight perturbation might force the stopped wave front to move again at an earlier time after $t = 2.5$ than this would happen for f_{stop} by unevitable numerical rounding errors.

Test 2; POD – initial control $0.99 \mathbf{f}_{\text{stop}}$. In the same way, we solved the reduced optimal control problems generated by POD. A comparison shows a very good coincidence between the FE solutions and the POD solutions. The reduced model was set up by 15 POD basis functions. We report on a few data:

Method	Hestenes-Stiefel	Fletcher-Reeves	Polak-Ribiere	Hager-Zhang
Optimal objective value	6.3283e-06	5.2063e-06	2.5737e-04	3.335e-06
Error $\ \bar{u} - \bar{u}^{\text{POD}}\ _{L^2(Q)}$	1.5179e-03	8.4226e-04	2.2508e-02	1.8802e-03
CPU time (in s)	150.72	103.29	37.58	101.25

TABLE 5.2

Test 2, Optimal objective values, CPU times, and estimated errors $\|\bar{u} - \bar{u}^{\text{POD}}\|_{L^2(Q)}$ by POD

On average, 0.2846s of the CPU time were used to set up the POD basis. Figure 5.11 shows the POD optimal solutions computed by the method of Hager and Zhang with $r = 15$ POD basis functions. As expected, graphically there is no difference to the solution obtained by f_{stop} . The CPU times for the POD model turned out to be longer than for the FE based full model. At first glance, this is surprising, but it has a simple explanation. In the POD model with $r = 15$ basis functions, the system matrices are fully populated. The effort for solving the linear systems per time step is of the order $r^3 = 3375$. In contrast to this, for the FEM the associated matrices are tri-diagonal with $m = 300$ elements in the diagonal. The numerical effort per time step is about $3m = 900$. Therefore, the longer running times for the POD model should not surprise. Nevertheless, the precision of the reduced model is remarkable. This indicates that reduced models should be helpful for higher space dimensions, where the computational effort of the FEM will be much larger.

Test 3; FEM – initial control $0.5 \mathbf{f}_{\text{stop}}$. Here, we took the control $f^0 = 0.5 f_{\text{stop}}$ as starting function for the conjugate gradient method. The optimal control, computed by the Polak-Ribiere version with strong Wolfe-Powell step size rule, is displayed in Fig. 5.12 (left-hand side). The

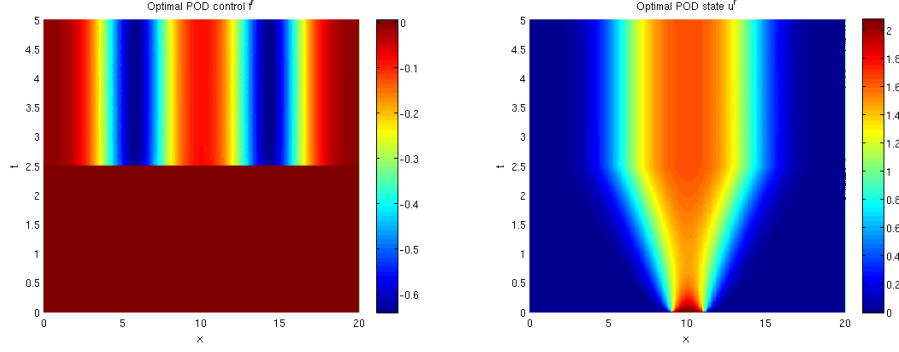


FIG. 5.11. *Test 2, Optimal control \bar{f}^{POD} (left) and optimal state \bar{u}^{POD} (right).*

associated optimal state does graphically not differ from the one shown in Figure 5.10. The optimal solutions of the POD model differ only marginally from them. Graphically the difference is not visible, therefore, we do not show the associated figures.

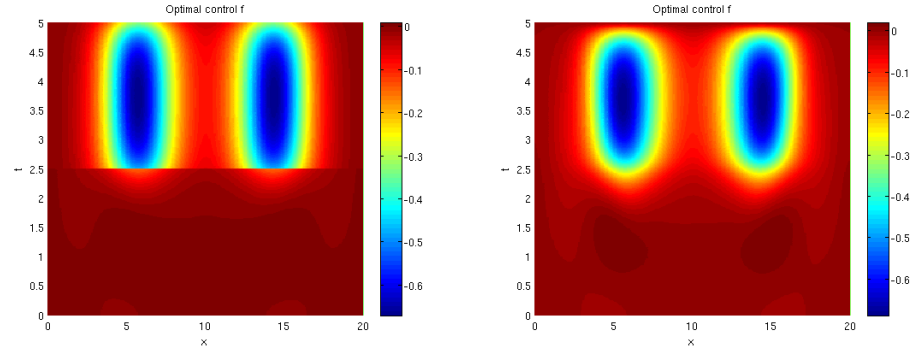


FIG. 5.12. *Optimal controls \bar{f} for Test 3 (left) and Test 4 (right).*

The optimal values of the objective function were $1.0997 \cdot 10^{-3}$ (FE model) and $7.5269 \cdot 10^{-4}$ (POD model). As CPU time, 99.52 s were needed for the optimization of the finite element model and 152.05 s for the POD model. The errors between the FE and POD optimal solutions are $\|\bar{f} - \bar{f}^{POD}\|_{L^2(Q)} = 3.46 \cdot 10^{-2}$, $\|\bar{u} - \bar{u}^{POD}\|_{L^2(Q)} = 1.1 \cdot 10^{-2}$, and $\|\bar{p} - \bar{p}^{POD}\|_{L^2(Q)} = 0.1104$.

Test 4 – initial control $\mathbf{f}_0 = \mathbf{0}$. Here, we started the cg method by $f^0 \equiv 0$. The optimal solutions are still satisfactory. The optimal objective values are $2.5959 \cdot 10^{-3}$ (FE model) and $4.8361 \cdot 10^{-3}$ (POD model) with CPU times 96.87 s (FE) 154.35 s (POD). The differences between the optimal states, controls and adjoint states are of the same order as in the last subsection. The optimal control is presented in Fig. 5.12 (right-hand side). Also here, the optimal state coincides graphically almost with that of Figure 5.10. The following deviations from the POD optimal solutions to the ones computed by FEM were determined:

$$\|\bar{f} - \bar{f}^{POD}\|_{L^2(Q)} = 0.12067, \quad \|\bar{u} - \bar{u}^{POD}\|_{L^2(Q)} = 3.3512 \cdot 10^{-2}, \quad \|\bar{p} - \bar{p}^{POD}\|_{L^2(Q)} = 0.20241.$$

Again, the results were obtained by the Polak-Ribiere version with strong Wolfe-Powell step size rule.

Test 5 – initial control $\mathbf{f}_0 = \mathbf{1}$. Computations with the initial control $f^0 \equiv 1$ did generate just acceptable results. Here an optimal value of $6.6556 \cdot 10^{-2}$ was achieved by the FE model and $3.892 \cdot 10^{-2}$ for the POD model with CPU times 94.19 s (FE) and 151.38 s (POD). The differences between FEM and POD optimal solutions were

$$\|\bar{f} - \bar{f}^{POD}\|_{L^2(Q)} = 0.3284, \|\bar{u} - \bar{u}^{POD}\|_{L^2(Q)} = 0.1557, \|\bar{p} - \bar{p}^{POD}\|_{L^2(Q)} = 1.9822$$

The computed optimal states approximate the desired ones fairly well. Moreover, the optimal states for the FE model and for the POD model show again a very good coincidence, cf. Fig. 5.13. The FE based solutions were computed by the nonlinear cg method of Polak-Ribiere with the strong Wolfe-Powell step size rule.

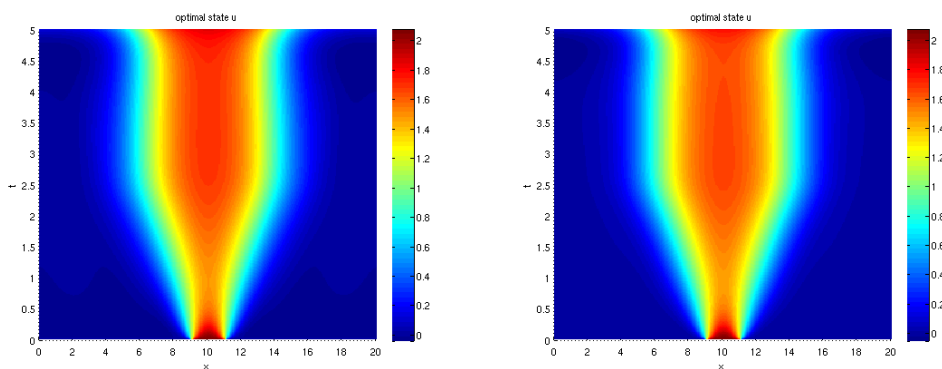


FIG. 5.13. Test 5, Optimal states: FE (left) and POD (right)

These 5 tests show that the convergence of the nonlinear cg method is fairly slow and sensitive with respect to the initial iterate. We did not observe such low performance for the semilinear heat equation with monotone nonlinearity. This seems to be a difficulty that is related to traveling waves. While this is not critical with respect to the approximation of the optimal states, significant deviations between the computed optimal controls arise. POD reduced models are able to determine the optimal solution with the same precision as the full finite element model.

Acknowledgement. The authors are very grateful to Christopher Ryll (TU Berlin, Institute of Mathematics), who updated and partially improved the numerical results of the third author after she finished her university career.

REFERENCES

- [1] H. Amann. *Linear and quasilinear parabolic problems. Vol. I*, volume 89 of *Monographs in Mathematics*. Birkhäuser Boston Inc., Boston, MA, 1995. Abstract linear theory.
- [2] E. Arian, M. Fahl, and E. W. Sachs. Trust-region proper orthogonal decomposition for flow control. Technical report, ICASE, 2000. Technical Report 2000-25.
- [3] F. Bonnans and E. Casas. Une principe de Pontryagine pour le contrôle des systèmes semilinéaires elliptiques. *J. Diff. Equations*, 90:288–303, 1991.

- [4] A. Borzi and R. Griese. Distributed optimal control of lambda-omega systems. *J. Numer. Math.*, 14(1):17–40, 2006.
- [5] E. Casas. Pontryagin’s principle for state-constrained boundary control problems of semilinear parabolic equations. *SIAM J. Control and Optimization*, 35:1297–1327, 1997.
- [6] E. Casas, J. C. De los Reyes, and F. Tröltzsch. Sufficient second-order optimality conditions for semilinear control problems with pointwise state constraints. *SIAM J. on Optimization*, 19(2):616–643, 2008.
- [7] S. Chaturantabut and D. C. Sorensen. Nonlinear model reduction via discrete empirical interpolation. *SIAM J. Sci. Comput.*, 32(5):2737–2764, 2010.
- [8] E. Di Benedetto. On the local behaviour of solutions of degenerate parabolic equations with measurable coefficients. *Ann. Scuola Sup. Pisa, Ser. I*, 13:487–535, 1986.
- [9] M. Fahl and E. W. Sachs. Reduced order modelling approaches to PDE-constrained optimization based on proper orthogonal decomposition. In L. T. Biegler, O. Ghattas, M. Heinkenschloss, and B. van Bloemen Waanders, editors, *Large-Scale PDE-Constrained Optimization*, volume 30, pages 268–280, Berlin, 2003. Springer-Verlag.
- [10] W. W. Hager and H. Zhang. CG DESCENT, a conjugate gradient method with guaranteed descent. Technical report, ACM TOMS, 2006.
- [11] W. W. Hager and H. Zhang. A survey of nonlinear conjugate gradient methods. *Pac. J. Optim.*, 2(1):35–58, 2006.
- [12] M. Heinkenschloss and E. W. Sachs. Numerical solution of a constrained control problem for a phase field model. In W. Desch, F. Kappel, and K. Kunisch, editors, *Control and Estimation of Distributed Parameter Systems*, volume 118 of *ISNM*, pages 171–188. Birkhäuser Verlag, 1994.
- [13] R. Herzog and K. Kunisch. Algorithms for PDE-constrained optimization. *GAMM-Mitt.*, 33(2):163–176, 2010.
- [14] M. Hinze, R. Pinnau, M. Ulbrich, and S. Ulbrich. *Optimization with PDE Constraints*, volume 23. Springer-Verlag, Berlin, 2009.
- [15] E. Kammann, F. Tröltzsch, and S. Volkwein. A method of a-posteriori estimation with application to proper orthogonal decomposition. *ESAIM: Mathematical Modelling and Numerical Analysis*, 47(2):555–581, 2013.
- [16] K. Kunisch and S. Volkwein. Galerkin proper orthogonal decomposition methods for parabolic problems. *Numerische Mathematik*, 90:117–148, 2001.
- [17] Karl Kunisch, Chamakuri Nagaiah, and Marcus Wagner. A parallel Newton-Krylov method for optimal control of the monodomain model in cardiac electrophysiology. *Comput. Vis. Sci.*, 14(6):257–269, 2011.
- [18] Karl Kunisch and Marcus Wagner. Optimal control of the bidomain system (II): Uniqueness and regularity theorems for weak solutions. *To appear in Annali di Matematica Pura ed Applicata*.
- [19] Karl Kunisch and Marcus Wagner. Optimal control of the bidomain system (III): Existence of minimizers and first-order optimality conditions. *To appear in ESAIM: Mathematical Modelling and Numerical Analysis*.
- [20] Karl Kunisch and Marcus Wagner. Optimal control of the bidomain system (I): the monodomain approximation with the Rogers-McCulloch model. *Nonlinear Anal. Real World Appl.*, 13(4):1525–1550, 2012.
- [21] Y. Kuramoto. *Chemical oscillations, waves, and turbulence*, volume 19 of *Springer Series in Synergetics*. Springer-Verlag, Berlin, 1984.
- [22] G. Leugering, S. Engell, A. Griewank, M. Hinze, R. Rannacher, V. Schulz, M. Ulbrich, and S. Ulbrich. *Constrained Optimization and Optimal Control for Partial Differential Equations*, volume 160 of *ISNM*. Birkhäuser Verlag, 2012.
- [23] J. Löber. Nonlinear excitation waves in spatially heterogenous reaction-diffusion systems. Technical report, TU Berlin, Institute of Theoretical Physics, 2009.
- [24] A. S. Michailov. *Foundations of Synergetics*, volume 1. Springer-Verlag, Berlin, 1994.
- [25] M. Müller. *Uniform convergence of the POD method and applications to optimal control*. Phd thesis, Johannes Kepler University Graz, 2011.
- [26] J. D. Murray. *Mathematical biology*, volume 19 of *Biomathematics*. Springer-Verlag, Berlin, second edition, 1993.
- [27] J.-P. Raymond and H. Zidani. Pontryagin’s principle for state-constrained control problems governed by parabolic equations with unbounded controls. *SIAM J. Control and Optimization*, 36:1853–1879, 1998.
- [28] F. Schlögl. A characteristic critical quantity in nonequilibrium phase transitions. *Z. Phys. B – Condensed Matter*, 52:51–60, 1983.
- [29] E. Schöll and H.G. Schuster. *Handbook of Chaos Control, 2nd Edition*. Wiley-VCH, Weinheim, 2008.
- [30] Joel Smoller. *Shock waves and reaction-diffusion equations*, volume 258 of *Grundlehren der Mathematischen Wissenschaften [Fundamental Principles of Mathematical Sciences]*. Springer-Verlag, New York, second edition, 1994.
- [31] F. Tröltzsch. *Optimal Control of Partial Differential Equations. Theory, Methods and Applications*, volume 112. American Math. Society, Providence, 2010.

- [32] S. Volkwein. Model reduction using proper orthogonal decomposition. Lecture notes, Institute of Mathematics and Scientific Computing, University of Graz, 2007.